Physica D 61 (1992) 289–296
North-Holland

PHYSICA D

# Three-dimensional dissipative structures in reaction–diffusion systems

A. De Wit, G. Dewel, P. Borckmans and D. Walgraef

*Service de Chimie-Physique and Centre for Nonlinear Phenomena and Complex Systems, C.P. 231, Université Libre de Bruxelles, 1050 Brussels, Belgium*

We study analytically and numerically the tridimensional pattern selection problem for reaction–diffusion systems. Qualitative agreement is found with the recent experimental results.

## 1. Introduction

Diffusion induced instabilities have been presented as the paradigm for modelling the onset of patterns in driven systems in fields as diverse as chemistry [1], biology [2,3] and materials science [4,5]. Among these, the Turing instability [6] that had been proposed in 1952 as the "Chemical Basis for Morphogenesis", has received special attention because of its biological relevance. This spontaneous space symmetry-breaking instability that arises solely from the interplay between diffusion and chemical reactions gives rise to stationary periodic concentration patterns, "chemical dissipative crystals". The beauty of Turing's idea lies in the fact that diffusion plays here a counter-intuitive role, leading to a spontaneous ordering of the system instead of smoothing all inhomogeneities. Since 40 years, a lot of theoretical and numerical analysis of reaction–diffusion models have corroborated the generality of such a structuring mechanism. The status of experimentation in the field was however far less satisfactory. Indeed, all the steady concentration patterns that had been previously reported in close reactors were due to convective or surface effects [7,12]. Furthermore, to maintain the system out of equilibrium, fresh reactants have to be injected continuously in the reactor interfering with the formation of the stationary pattern. Besides, the conditions of appearance of these structures (e.g. the different chemical species should diffuse at different rates) are rarely fulfilled in the commonly used aqueous solutions of non linear chemical reactions. More recently, the design of open "gel reactors" [8–11] has finally allowed the observation of the first sustained steady "chemical dissipative crystals" in the chlorite-iodide-malonic acid (CIMA) reaction [8,9]. The reaction takes place in a thin flat piece of permeable inert gel, two opposite edges of which are in contact with open chemical reservoirs of different well-controlled compositions. The experimental results may be divided into two series depending on the orientation of the feeding of the gel:

– Ouyang et al. [9] report the case where the vizualisation is parallel to the feeding direction. According to the value of the parameters, extended quasi-twodimensional (2D) concentration patterns in the form of bands or hexagons are observed. A large number of defects (dislocations and disclinations) resulting from the nucleation processes are present in these chemical

structures presenting striking similarities with the numerous examples of structurations observed in hydrodynamical systems.

– In another set of experiments performed by Castets et al. [8], the vizualisation is perpendicular to the feeding direction. When the control parameter of the experiment becomes higher than a given threshold, a breaking of the feeding's symmetry appears through dots organized as an hexagonal pattern. Because of the presence of concentration gradients, this pattern is *localized* in a subregion of the reactor. Besides, as the wavelength of the pattern is smaller ($\approx 200\,\mu$m) than any geometric size of the system, these structures are actually *three-dimensional* (3D). Contrary to the well studied hydrodynamic instabilities one must therefore deal with the full 3D pattern selection problem [13–15]. We do so in the weakly nonlinear regime, when $\mu$, the distance from the bifurcation point is small and for a uniform feeding (pool chemical approximation). Here we describe the competition among the possible 3D structures and use these analytical solutions to put our numerical results on a reaction–diffusion model into proper perspective. The resulting patterns present close similarities with those obtained experimentally.

## 2. Pattern selection

The basic equations for Turing's reaction-diffusion mechanism can be written in the form

$$\frac{\partial \boldsymbol{C}}{\partial t} = \boldsymbol{f}(\boldsymbol{C}) + \boldsymbol{D}\nabla^2 \boldsymbol{C}\,,$$

where $\boldsymbol{C}$ is a vector of concentrations, $\boldsymbol{f}$ represents the reaction kinetics and $\boldsymbol{D}$ is the diagonal matrix of positive diffusion coefficients. The kinetics in any practical situation is always nonlinear. The relevant initial and boundary conditions should be added to this system. If, in the absence of diffusion, $\boldsymbol{C}$ tends to a linearly stable uniform state $\boldsymbol{C}_0$ then, under certain conditions, spatially inhomogeneous periodic patterns can evolve by a diffusion driven instability if the diffusion coefficients are different.

For *extended* (of size much larger than the wavelength of the structure) isotropic systems, as are chemical systems in liquid solutions, the linear stability analysis shows that all perturbations of $\boldsymbol{C}_0$ with wavevectors $\boldsymbol{k}$ such that $|\boldsymbol{k}| = k_c$ are equally amplified at $\mu = 0$. The competition among the various excited modes that arise because of this *orientational degeneracy* can be studied by considering the various superpositions of such modes [16]

$$\boldsymbol{C}(\boldsymbol{r}, t) = \boldsymbol{C}_0 + \sum_{i=1}^{m} (A_i\, \mathrm{e}^{\mathrm{i}\boldsymbol{k}_i\cdot\boldsymbol{r}} + A_i^*\, \mathrm{e}^{-\mathrm{i}\boldsymbol{k}_i\cdot\boldsymbol{r}})\,,$$

$$|\boldsymbol{k}_i| = k_c\,,$$

where $A_i = R_i\, \mathrm{e}^{\mathrm{i}\phi_i}$ is the complex amplitude of the excited mode with wavevector $\boldsymbol{k}_i$. Each pattern is thus characterized by $m$ *pairs* of wavevectors.

Using the standard techniques of bifurcation analysis [1,17] leads to the following equations determining the amplitudes $A_i$ (in absence of spatial modulation):

$$\frac{\mathrm{d}A_i}{\mathrm{d}t} = \mu A_i + v \sum_j \sum_k A_j^* A_k^* \delta(\boldsymbol{k}_i + \boldsymbol{k}_j + \boldsymbol{k}_k)$$

$$-|A_i|^2 A_i - \sum_j \gamma_{ij} |A_j|^2 A_i$$

$$-\sum_j \sum_k \sum_l \beta_{jkl} A_j^* A_k^* A_l^* \delta(\boldsymbol{k}_i + \boldsymbol{k}_j + \boldsymbol{k}_k + \boldsymbol{k}_l)\,.$$

The coefficients $\gamma_{ij}$ are functions of the angle $\theta_{ij}$ between the wavevectors $\boldsymbol{k}_i$ and $\boldsymbol{k}_j$. The simplest solution to this equation ($m = 1$) represents a smectic-like ordering of lamellae (or walls). For $m = 2$, one has a set of two intersecting lamellae systems. A section, parallel to $\boldsymbol{k}_1 \times \boldsymbol{k}_2$, yields a lattice of rhombs. As we assume here, in relation with the numerical results to be presented, that $\gamma_{ij}(\theta) > 1$ for all $\theta$, this $m = 2$ structure is un-

stable. The case $m = 3$: $\boldsymbol{k}_1 + \boldsymbol{k}_2 + \boldsymbol{k}_3 = 0$, corresponds to a rodlike structure with 2D hexagonal symmetry. For $m = 4$, the basic wavevectors can be arranged to form a non-coplanar quadrangle ($\boldsymbol{k}_1 + \boldsymbol{k}_2 + \boldsymbol{k}_3 + \boldsymbol{k}_4 = 0$). The $\gamma_{ij}(\theta) > 1$ condition also insures the lack of stability of the triperiodic patterns built on non-coplanar wavevectors (leading to sc and fcc lattices). When $m = 6$, the basic wavevectors are parallel to the edges of a regular octahedron, each vector participating in two triangles. The corresponding structure in real space has a body centered cubic symmetry (bcc). The study of the relative stability of these patterns allows us to draw the bifurcation diagram (see fig. 1) associated to the stability limits of these structures given in table 1. On increasing the value of $\mu$ the following sequence of patterns may thus emerge: a bcc structure for the maxima of concentrations is the first to appear subcritically. It is followed, also subcritically, by hexagonal prisms and then supercritically by lamellae. The stability limit points are furthermore interconnected by unstable mixed mode branches. Reversing the variation of the bifurcation parameter one backtracks through the various structures but by undergoing hysteresis loops at each transition. Thus for a wide range of values of the parameters various structures may coexist and the system may even exhibit *spatial tristability*. The degree of subcriticality may be shown to be small with respect to the stability domain in agreement with the experiments [9].

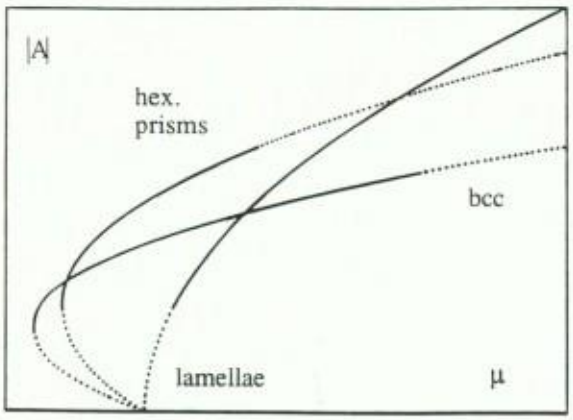


Fig. 1. Bifurcation diagram in 3D. Full and dotted lines represent respectively stable and unstable steady states.

One should however bear in mind that sufficiently far beyond the threshold higher order terms come into play in eq. [2]. They may alter the nature of the stable solutions for high $\mu$ and furthermore could lead to quasiperiodic structures with for instance local fivefold symmetry [18].

## 3. Numerical results

These predictions have been checked in a series of 3D numerical integrations of the equations of the Brusselator model that has been extensively used in studies of chemical dissipative structures [1]. The choice of this model is by

Table 1
Stability regions of the 3D structures.

| Structure | Domain of stability |
|---|---|
| bcc lattice ($m = 6$) | $-\dfrac{v^2}{[4\gamma(2\pi/3) + \gamma(\pi/2) + 1]} \le \mu \le \dfrac{v^2[4\gamma(2\pi/3) - \gamma(\pi/2) + 3]}{[\gamma(\pi/2) - 1]^2}$ |
| hex prisms ($m = 3$) | $-\dfrac{v^2}{[8\gamma(2\pi/3) + 4]} \le \mu \le \dfrac{v^2[\gamma(2\pi/3) + 2]}{[\gamma(2\pi/3) - 1]^2}$ |
| lamellae ($m = 1$) | $\dfrac{v^2}{[\gamma(2\pi/3) - 1]^2} \le \mu$ |

no means a restriction to the generality of the results. Indeed, the particularities of a specific model affect only the precise values of the thresholds and the relative widths of stability regions and not the succession of structures in a particular scenario.

In terms of scaled variables the corresponding equations take the form

$$\frac{\partial X}{\partial t} = A - (B+1)X + X^2Y + D_x\nabla^2 X\,,$$

$$\frac{\partial Y}{\partial t} = BX - X^2Y + D_y\nabla^2 Y\,,$$

where $A$ and $B$ are the control pool species and the concentration of $B$ is taken as the bifurcation parameter. This system exhibits a Turing instability at $B = B_c = [1 + A\sqrt{D_x/D_Y}]^2$ with $k_c^2 = A/\sqrt{D_X D_Y}$ when $D_Y > D_X A^2/(\sqrt{1+A^2}-1)^2$.

In 2D, this model exhibits hexagons and rolls. In large systems, we have also observed the presence of defects (see fig. 2) analog to those observed in the extended quasi-2D experimental results.

In 3D and for the values of the parameters given in the captions, numerical integrations lead, on increasing B, to the theoretically predicted succession of structures: bcc, hexagonal prisms and lamellae (figs 3–5).

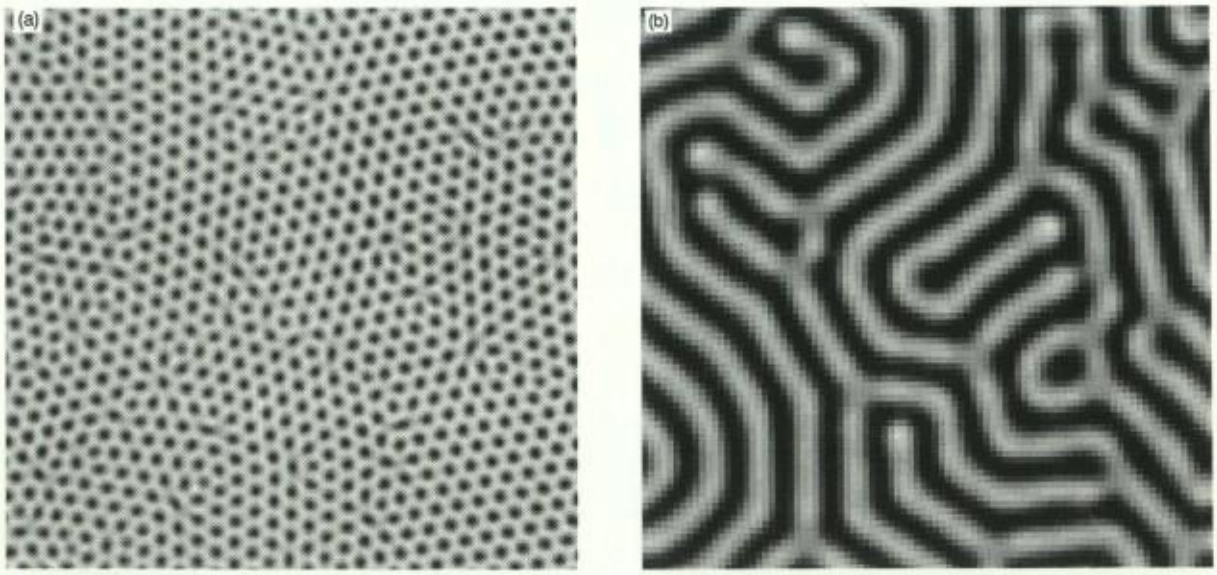


Fig. 2. Examples of 2D patterns for the concentration of species $X$ in the Brusselator in an extended system. The integrations were carried out on a square grid of size $256 \times 256$ in (a) and $90 \times 90$ in (b) imposing periodic boundary conditions. As the integration is started from random initial conditions, the orientational degeneracy leads to the formation of competing patches. Their compatibility is solved through the generation of defects. These patterns remain time dependent over very long times (driven by the slow evolution of the phases $\phi_i$) and indeed may never settle down at all. The parameters are $A = 4.5$, $D_X = 2.8$, $D_Y = 22.4$ and $B$ is respectively 7.1 for the "hexagonal" (a) and 8.0 for the "striped" structure (b). The wavenumber is of the order of $k_c$. The defects are respectively of the hepta-pentagon pair (a) and disclination (b) types. As these patterns present no further structuration when extended to 3D, they are relevant to the interpretation of the experimental results if only their alignment with respect to the imposed feeding gradient is correct. This analysis remains to be done.

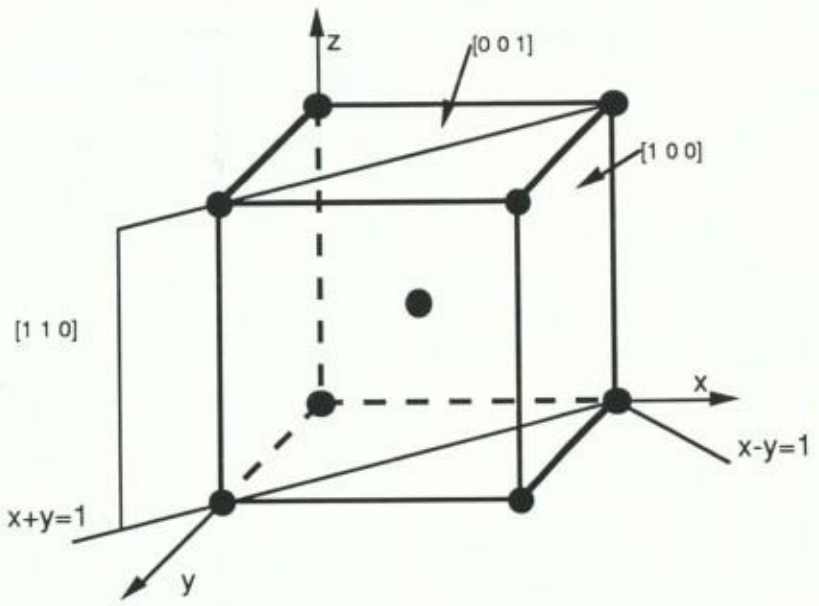


(a)

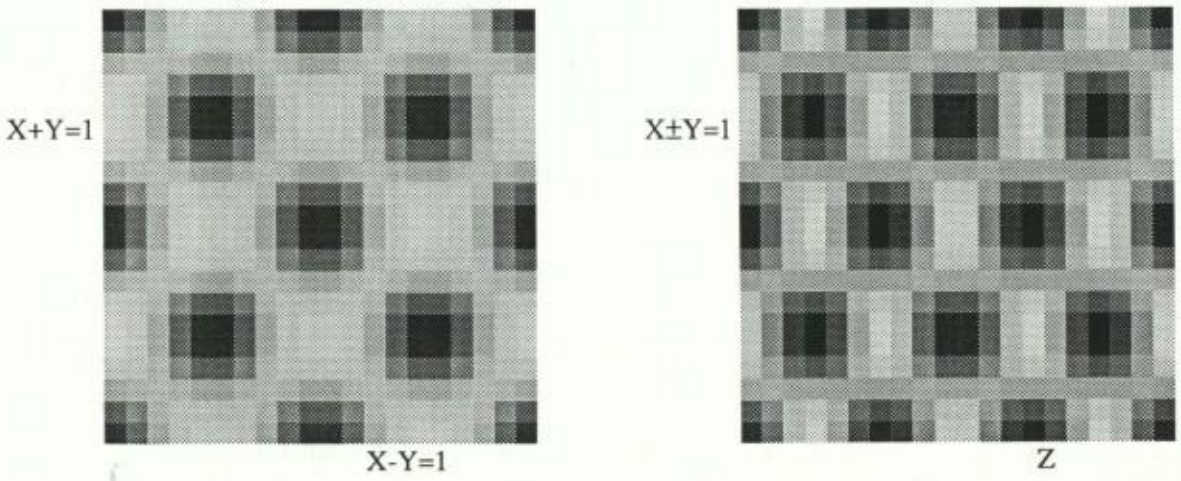


(b) [0 0 1] (c) [1 1 0] or [1 $\bar{1}$ 0]

Fig. 3. Stable stationary 3D pattern with bcc symmetry for the concentration of species $X$ in the Brusselator (Eq. 3). The darker and lighter shades respectively represent minima and maxima of concentrations with respect to the reference uniform state ($X_0 = A$, $Y_0 = B/A$). The integration of eq. (3) was performed on a $20 \times 20 \times 20$ grid imposing periodic boundary conditions on each face of the cube. Selected modes are excited in the initial condition in order to partially orient the resulting structure for visualization purposes. The chosen initial condition leads to a bcc structure rotated by $\pi/4$ around the $z$ axis. The parameters are $A = 4.5$, $D_X = 1$, $D_Y = 8$ (thus $B_c = 6.71$) and $B = 6.8$ ($\mu \approx 0.0134$). (a) Schematic representation of the bcc primitive cell serving as a visualization aid. (b), (c) The symmetry of the structure obtained by integration is made explicit by exhibiting three characteristic orthogonal planes noted by their Miller indices. The wavenumber is of the order of $k_c$.

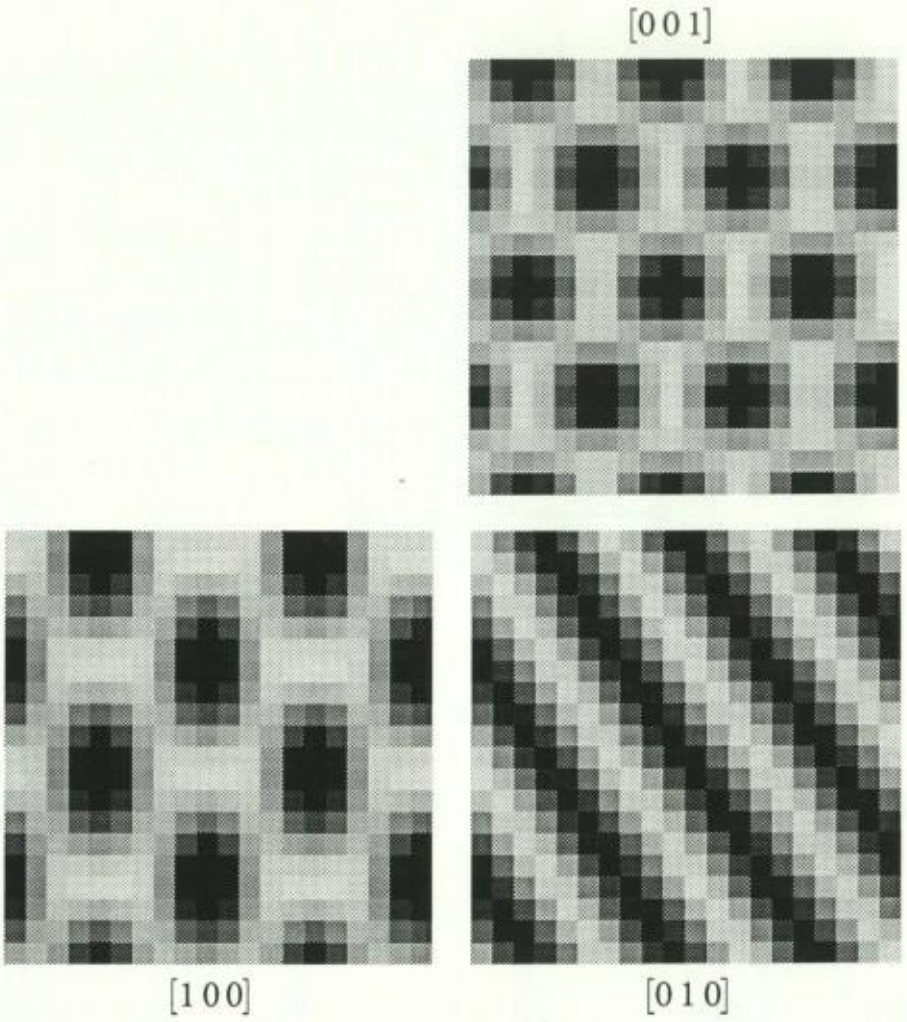


Fig. 4. A 3D pattern of hexagonal prisms for the concentration of species $X$ for the Brusselator obtained as in fig. 3 for $B = 7.0$ ($\mu \approx 0.043$). The initial conditions give rise to hexagonal prisms that are inclined by $\pi/4$ with respect to the $z$ axis. The structure is made explicit by showing the ordering in the three planes [100], [010] and [001].

## 4. Conclusions

Our numerical simulations of the Brusselator model have thus shown the theoretically predicted succession of patterns in 3D and present striking similarities with the experimentally produced structures. However the experimental patterns are obtained in the presence of concentration gradients of the control species, due to the feeding of the reactor, and are thus of the *localized* type [19,20]. Interestingly such a localized pattern was also obtained for a realistic model of the CIMA reaction in 1D space [21]. We have nevertheless also obtained all the above discussed 3D structures in the presence of gradients such as those due to lateral feeding fluxes. For some conditions the three structures may even coexist spatially in the system, each appearing in the region where the bifurcation parameter $B$ locally exceeds the corresponding threshold

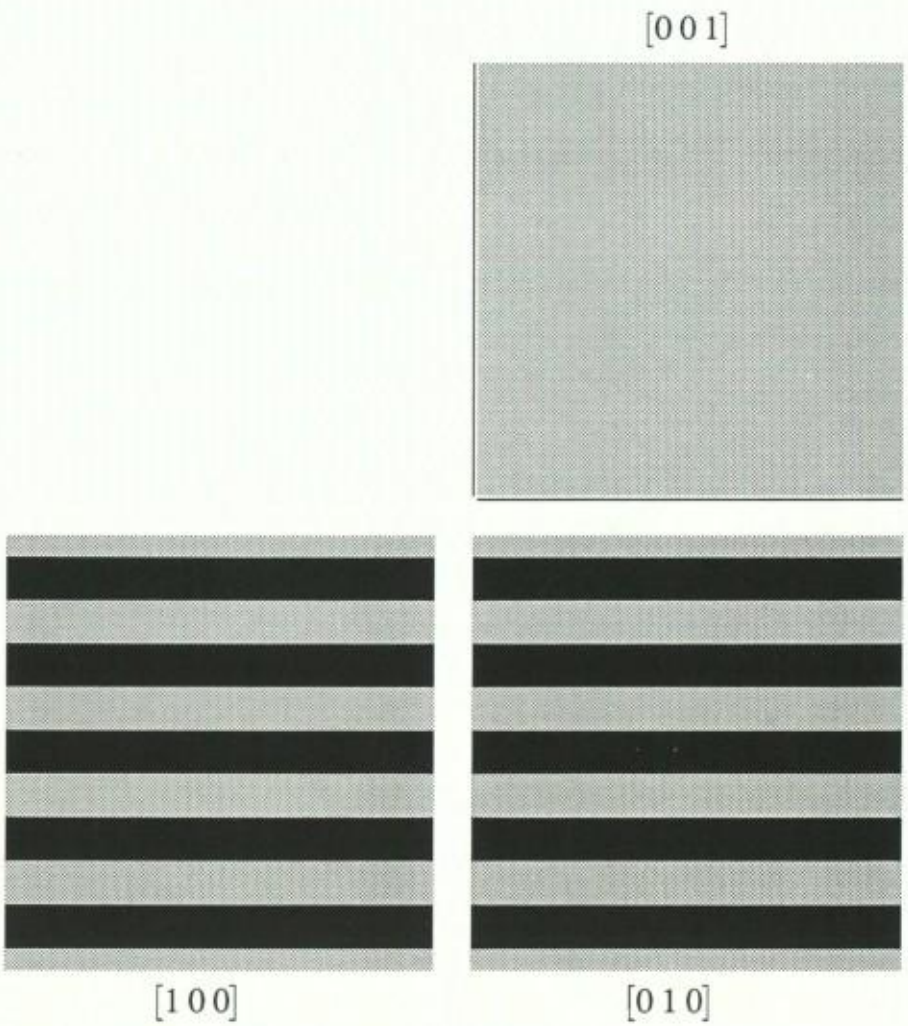


Fig. 5. A 3D pattern of lamellae for the concentration of species $X$ for the Brusselator when $B = 8.5$ [$\mu \approx 0.267$]. The representation is as in fig. 4. The sharpness of the transition between the regions of high and low concentrations as attested by the color scales (hence the name lamellae) is related to the high content in harmonics because $\mu$ is already large.

and separated by transition fronts of complex nature.

We may thus conclude that the analytical and numerical results pave the way to a large understanding of the experimental phenomena. The study of the pattern selection and orientation with respect to such gradients [22–25], that partially lift the orientational degeneracy, is under study. The nature and the role of 3D fronts and defects in the transition between structures of different symmetries or in the disorganization of such patterns remain to be assessed.

**Acknowledgements**

We thank I. Prigogine and G. Nicolis for their interest in this work and A. Arneodo, J. Boissonade, P. De Kepper, Q. Ouyang and H. Swinney for stimulating discussions. P.B. and G.D.

are Senior Research Assistant and D.W. is Research Associate with the F.N.R.S. (Belgium). A.D. is I.R.S.I.A. (Belgium) fellow.

## References

[1] G. Nicolis and I. Prigogine, Self-Organization in Nonequilibrium Systems (Wiley, New York, 1977).
[2] H. Meinhardt, Models of Biological Pattern Formation (Academic Press, New York, 1982).
[3] J.D. Murray, Mathematical Biology (Springer, Berlin, 1989).
[4] K. Krishan, Nature 287 (1980) 420.
[5] D. Walgraef and N.M. Ghoniem, Phys. Rev. B 13 (1990) 8867.
[6] A. Turing, Phil. Trans. R. Soc. Lond. 237B (1952) 37.
[7] P. Borckmans, G. Dewel, D. Walgraef and Y. Katayama, J. Stat. Phys. 48 (1987) 1031.
[8] V. Castets, E. Dulos, J. Boissonade and P. De Kepper, Phys. Rev. Lett. 64 (1990) 2953.
[9] Q. Ouyang and H.L. Swinney, Nature 352 (1991) 610.
[10] Z. Noszticzius, W. Horsthemke, W.D. McCormick, H.L. Swinney and W.Y. Tam, Nature 329 (1987) 619.
[11] G. Kshirsagar, Z. Noszticzius, W.D. McCormick and H.L. Swinney, Physica D 49 (1991) 5.
[12] J-C. Micheau, M. Gimenez, P. Borckmans and G. Dewel, Nature 305 (1983) 43.
[13] G. Dewel, P. Borckmans and D. Walgraef, J. Phys. C 12 (1979) L491.
[14] D. Walgraef, G. Dewel and P. Borckmans, Adv. Chem. Phys. 49 (1982) 311.
[15] P. Borckmans, G. Dewel and A. De Wit, Rev. Cytol. Biol. Végét. Bot. 14 (1991) 139.
[16] F.H. Busse, Rep. Prog. Phys. 41 (1978) 1929.
[17] P. Manneville, Dissipative Structures and Weak Turbulence (Academic Press, Boston, 1990).
[18] D. Walgraef, G. Dewel and P. Borckmans, Nature 318 (1985) 606.
[19] M. Herschkowitz-Kaufman and G. Nicolis, J. Chem. Phys. 56 (1972) 1890.
[20] P. Ortoleva and J. Ross, J. Chem. Phys. 56 (1972) 4397.
[21] I. Lengyel and I.R. Epstein, Science 251 (1991) 650.
[22] T.C. Lacalli, D.A. Wilkinson and L.C. Harrison, Development 104 (1988) 105.
[23] D. Walgraef and C. Schiller, Physica D 27 (1987) 423.
[24] G. Dewel and P. Borckmans, Phys. Lett. A 138 (1989) 189.
[25] A. Hunding and M. Brøns, Physica D 44 (1990) 285.